Available online at www.sciencedirect.com
SCIENCE DIRECT
Chemical Physics 323 (2006) 193–203
Chemical Physics
www.elsevier.com/locate/chemphys

The structure of low-index surfaces of β-Ga_2O_3

V.M. Bermudez *

Electronics Science and Technology Division, Naval Research Laboratory, Code 6876, 4555 Overlook Avenue, S.W., Washington, DC 20375-5347, United States

Received 13 July 2005; accepted 25 August 2005
Available online 18 October 2005

Abstract

The physical and electronic structure of the (1 0 0), (0 1 0), (0 0 1) and (1 0 $\bar{1}$) faces of β-Ga_2O_3 are addressed using ab initio theory. Restricted Hartree–Fock calculations, with large-core Ga and O pseudopotentials, are done to optimize the structure of first the bulk and then of slabs "cut" in the required orientations. The slab unit cells are fully relaxed during optimization, and the displacements of all atoms from the ideally-terminated positions are obtained as functions of depth into the bulk. For the relaxed slabs, single-point density functional theory calculations using the B3LYP functional and all-electron basis sets are performed to obtain surface energies, ionic charges and bond overlap populations. All surfaces exhibit a decrease in surface energy upon relaxation, and the local bonding at the surface is analyzed by comparing nearest-neighbor bond lengths and overlap populations with those in the bulk. The (1 0 $\bar{1}$) surface, which exhibits a high energy when ideally terminated, undergoes large displacements and changes in bonding during relaxation leading to a substantial lowering of the surface energy. The band structure is also obtained for the lowest-energy surface, which is one of the possible non-polar terminations of the (1 0 0). The results provide insight into the growth and structure of β-Ga_2O_3 nanoribbons.
Published by Elsevier B.V.

Keywords: Density functional theory; Surface structure; Surface energy; Gallium oxide; Hartree–Fock; Nanoribbons

1. Introduction

Monoclinic gallium oxide (β-Ga_2O_3) has a number of interesting bulk and surface properties. When doped (e.g., with Sn) it can be used to form an ultraviolet-transmitting (band gap, E_g, ~4.5–4.9 eV) conducting layer [1]. Thin films of polycrystalline β-Ga_2O_3 containing O vacancies have long been known as sensors for a variety of gases including H_2 [2], CH_4 [3], CO [4] and O_2 [5] which change the electrical conductivity upon adsorption. A further source of interest in Ga_2O_3 surfaces is the recent work on nanowires and nanoribbons (or nanobelts) [6]. Nanoribbons grow as single crystals, typically along the [0 1 0] [7–9] or [0 0 1] [9–11] directions; although, there have been reports of growth along the [111] [12], [1 1 0] [13] or [1 0 $\bar{1}$] [14] directions.[1] The nanoribbons have well-defined surface planes. Growth in the [0 0 1] direction gives ribbons enclosed by ±(1 0 0) and ±(0 1 0) planes, while ribbons grown in the [0 1 0] direction have sides that are ±(1 0 0) and ±(1 0 $\bar{1}$) [6,9]. In either case, the wide surfaces of the ribbon are ±(1 0 0). Single crystals of β-Ga_2O_3 cleave readily [15,16] on the (1 0 0) plane which suggests that this is the most stable surface.

Furthermore, powdered Ga_2O_3 is of interest in catalysis, and several studies have used the infrared absorption [17–19] or electron spin resonance [20] spectra of adsorbates on β-Ga_2O_3 powders, activated by evacuation at elevated temperature, as probes of the surface structure. The general conclusion is that such surfaces exhibit comparable densities of unsaturated tetrahedral and octahedral Ga sites (see below) and that the former are responsible for the

* Tel.: +1 202 767 6728; fax: +1 202 767 1165.
E-mail address: bermudez@estd.nrl.navy.mil.

[1] Care must be taken in reading papers referencing the β-Ga_2O_3 crystal structure. Some, such as [14], use a definition of the unit-cell axes that differs from the "standard" convention given below.

0301-0104/$ - see front matter. Published by Elsevier B.V.
doi:10.1016/j.chemphys.2005.08.051

Report Documentation Page

Form Approved
OMB No. 0704-0188

1. REPORT DATE	2. REPORT TYPE	3. DATES COVERED
JUL 2005		**00-00-2005 to 00-00-2005**

4. TITLE AND SUBTITLE	5a. CONTRACT NUMBER
The structure of low-index surfaces of b-Ga2O3	5b. GRANT NUMBER
	5c. PROGRAM ELEMENT NUMBER
6. AUTHOR(S)	5d. PROJECT NUMBER
	5e. TASK NUMBER
	5f. WORK UNIT NUMBER
7. PERFORMING ORGANIZATION NAME(S) AND ADDRESS(ES) **Naval Research Laboratory,4555 Overlook Avenue SW,Washington,DC,20375**	8. PERFORMING ORGANIZATION REPORT NUMBER
9. SPONSORING/MONITORING AGENCY NAME(S) AND ADDRESS(ES)	10. SPONSOR/MONITOR'S ACRONYM(S)
	11. SPONSOR/MONITOR'S REPORT NUMBER(S)

12. DISTRIBUTION/AVAILABILITY STATEMENT
Approved for public release; distribution unlimited

13. SUPPLEMENTARY NOTES

14. ABSTRACT

The physical and electronic structure of the (1 0 0), (0 1 0), (0 0 1) and ?1 0 1?faces of b-Ga2O3 are addressed using ab initio theory. Restricted Hartree?Fock calculations, with large-core Ga and O pseudopotentials, are done to optimize the structure of first the bulk and then of slabs ??cut?? in the required orientations. The slab unit cells are fully relaxed during optimization, and the displacements of all atoms from the ideally-terminated positions are obtained as functions of depth into the bulk. For the relaxed slabs, single-point density functional theory calculations using the B3LYP functional and all-electron basis sets are performed to obtain surface energies, ionic charges and bond overlap populations. All surfaces exhibit a decrease in surface energy upon relaxation, and the local bonding at the surface is analyzed by comparing nearest-neighbor bond lengths and overlap populations with those in the bulk. The ?1 0 1?surface which exhibits a high energy when ideally terminated, undergoes large displacements and changes in bonding during relaxation leading to a substantial lowering of the surface energy. The band structure is also obtained for the lowest-energy surface, which is one of the possible non-polar terminations of the (1 0 0). The results provide insight into the growth and structure of b-Ga2O3 nanoribbons.

15. SUBJECT TERMS

16. SECURITY CLASSIFICATION OF:			17. LIMITATION OF ABSTRACT	18. NUMBER OF PAGES	19a. NAME OF RESPONSIBLE PERSON
a. REPORT	b. ABSTRACT	c. THIS PAGE			
unclassified	**unclassified**	**unclassified**	**Same as Report (SAR)**	**11**	

Lewis-acid character of the activated β-Ga_2O_3 powders. In addition, studies of the thermal oxidation, in dry air or O_2, of hexagonal GaN epitaxial films [21,22] powders [22] or nanowires [23] have identified β-Ga_2O_3 as the resulting surface phase. The structure, stability and chemical properties of the oxide are significant factors in the subsequent processing of GaN substrates for device fabrication.

In view of this rich array of properties and applications it appears worthwhile to consider in detail the surface structure of β-Ga_2O_3. Experimental studies of the growth and ordering of well-characterized β-Ga_2O_3 films have been reported by Franchy and co-workers [24–30] for thin films formed by oxidation of the surfaces of the crystalline bimetallic compound CoGa. The only theoretical studies of β-Ga_2O_3 surfaces of which we are aware are those of Kohl et al. [31] and Gonzalez et al. [32] (discussed below) which employed semi-empirical cluster treatments to examine the adsorption of CH_4 and H, respectively, on (1 0 0) surfaces. In the present work, ab initio calculations will be done to study the structure and charge distribution of low-index surface planes of β-Ga_2O_3 since, as is already known [33], the Ga_2O_3 surface structure can have a pronounced effect on reactivity. Attention is focused on the (1 0 0), (0 1 0), (0 0 1) and $(1\,0\,\bar{1})$ faces since, as noted above, these appear to be among the most technologically important. There has, to our knowledge, been no previous theoretical or experimental work aimed at comparing the structure and properties of these low-index β-Ga_2O_3 surface planes.

2. Computational details

The large number of atoms and low symmetry of the unit cell (see below) make the computation demanding in terms of machine time. Therefore, geometry optimizations were performed using a restricted Hartree–Fock (RHF) approach with Durand–Barthelat large-core pseudopotentials. The electronic properties of the optimized structures were then obtained using density functional theory (DFT) with all-electron basis sets. Except where noted, all calculations were done using the CRYSTAL2003 suite of programs [34,35] which uses Bloch functions constructed from localized Gaussian basis sets. Two-dimensionally-periodic slabs, designed to maintain the symmetry and stoichiometry of the bulk unit cell, were used to model the various surfaces. The possible role of adsorbates and/or defects in stabilizing polar or non-stoichiometric surfaces [36] was not examined. Since localized, rather than plane-wave, basis sets were used there was no need to impose periodicity along the surface normal.

Optimization of the basis sets and the unit-cell lattice constants was done using the LoptCG script,[2] which computes gradients numerically using CRYSTAL98, followed by the application of a conjugate-gradient algorithm to locate the total-energy minimum. Optimization of the positions of individual atoms was done using CRYSTAL2003 which obtains energy gradients analytically. The single-point DFT calculations used the hybrid B3LYP functional which has been shown [37,38] to provide more accurate band gaps than do purely ab initio functionals.

The pseudopotential basis sets are given elsewhere.[3] For the Ga 21G* set, the exponents of the outer sp and d shells were re-optimized for Ga_2O_3, giving 0.2633 and 0.2930 $bohr^{-2}$ respectively. For the O 41G set, re-optimization of the outer sp exponent gave 0.2178 $bohr^{-2}$. The Ga all-electron basis set was the 86-4111d41G with the exponents of the outer three sp and one d shells re-optimized to 1.8605, 0.7105, 0.2775 and 0.6815 $bohr^{-2}$, respectively. The O all-electron basis set was the 8-411d1G with the exponents of the outer two sp and one d shells re-optimized to 0.4727, 0.1985 and 0.4497 $bohr^{-2}$, respectively.

The k-point sampling used an $8\times8\times6$ grid for the bulk and $8\times6\times1$, $6\times2\times1$, $8\times4\times1$ and $8\times2\times1$ grids for the (1 0 0)-, (0 1 0)-, (0 0 1)- and $(1\,0\,\bar{1})$-(1×1) slabs, respectively. In treating (2×2) slab supercells, for the purpose of including longer-range interactions, the k-point grid was reduced by a factor of 2 (e.g., a $4\times3\times1$ grid for the (1 0 0)-(2×2) slab). The interval in any case was in the range of 0.10–0.14 $bohr^{-1}$ per point. In CRYSTAL, truncation of the sums of Coulomb and exchange terms in the Fock matrix is determined by five overlap criteria (T1–T5) [34,35]. These were set at 10^{-7} for T1–T4 and 10^{-14} for T5. For integrals involving pseudopotentials the truncation criterion was typically set at 10^{-7}. In the multipolar expansion zone [34,35] a maximum order of $L=6$ was used. For the DFT calculations a Fock mixing of 50%, a Fermi-level smearing of 2×10^{-3} Hartrees and a level shift of 5 Hartrees were typically used in order to aid self-consistent field (SCF) convergence.

3. Results and discussion

3.1. Bulk properties

The most stable polymorph of Ga_2O_3 is the monoclinic β form which belongs to the C2/m (or C_{2h}^3) space group (number 12) with lattice parameters and atom positions given in Table 1 [39,40]. In the "standard" setting, which is used here, the b-axis of the centrosymmetric unit cell is the twofold rotational axis, and the mirror plane (i.e., the (0 1 0)) is perpendicular to this axis. There are four Ga_2O_3 units per crystallographic unit cell (which comprises two primitive unit cells) with two inequivalent Ga sites and three inequivalent O sites. Half the Gas are in Ga(I) sites which form slightly distorted tetrahedra with four O ions,

[2] The LoptCG script was obtained at http://www.crystal.unito.it/. At present, the publicly-available version of the script works only with CRYSTAL98. The latest version, CRYSTAL2003, can generate gradients analytically but only for the positions of individual atoms, not for basis-set parameters or lattice constants.

[3] The basis sets (both pseudopotential and all-electron) with full documentation are given at http://www.crystal.unito/it/Basis_Sets.

Table 1
Observed and calculated structural parameters for β-Ga_2O_3

Parameter	Calculated[a]	Experimental[b]
a	12.202 Å	12.23 ± 0.02
b	3.035 Å	3.04 ± 0.01
c	5.799 Å	5.80 ± 0.01
β	103.70°	103.7 ± 0.3
Ga(I)[c]	$x = 0.08981$; $z = -0.20723$	$x = 0.0904$; $z = -0.2052$
Ga(II)	0.34195; −0.31567	0.3414; −0.3143
O(I)	0.15754; 0.10867	0.1674; 0.1011
O(II)	0.49553; 0.25810	0.4957; 0.2553
O(III)	0.82544; 0.43290	0.8279; 0.4365

[a] This work, obtained in an RHF/pseudopotential calculation (see text). The crystallographic unit-cell volume is 208.65 Å^3.
[b] Results given by Geller [39, Table II]. The unit-cell volume is 209.50 Å^3. These values have been revised slightly by Åhman et al. [40].
[c] The atoms are all at the 4*i* special positions of the C2/m space group, given by $(0,0,0;\ 1/2,1/2,0) \pm (x0z)$. For each inequivalent site the values of x and z are given.

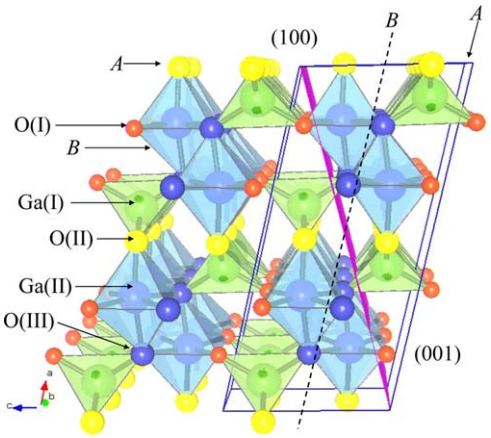

Fig. 1. The β-Ga_2O_3 lattice viewed along the (0 1 0) direction. The different inequivalent atom types are labeled. The labels "A" and "B" indicate the different (1 0 0) and (0 0 1) surface terminations (see text), and the dashed line shows the (0 0 1)-B plane. The box shows the unit cell, and the diagonal plane is the $(1\ 0\ \bar{1})$. The slightly different sizes shown for the two different Gas and for the three different Os are not significant.

and the other half are in Ga(II) sites which form highly distorted octahedra with six O ions. Each O(I) is threefold coordinated and lies at the intersection of two octahedra and one tetrahedron. Each O(II) is also threefold coordinated and is shared between one octahedron and two tetrahedra. Each O(III) is fourfold coordinated and lies at the corner of three octahedra and one tetrahedron. Fig. 1 shows a model of the lattice,[4] which illustrates the structural details noted above. In terms of the crystallographic unit cell vectors **a**, **b** and **c**, the primitive unit cell vectors are given by $\mathbf{a}' = (\mathbf{a} - \mathbf{b})/2$, $\mathbf{b}' = (\mathbf{a} + \mathbf{b})/2$ and $\mathbf{c}' = \mathbf{c}$.

Table 1 gives the lattice constants and atom positions obtained in the present work using the RHF/pseudopotential structural optimization described above. The optimization was done iteratively by alternately refining the lattice constants and the atom positions in separate calculations until convergence was achieved. The calculated structure is seen to be in good agreement with experiment. Table 2 gives the various Ga–O nearest-neighbor distances, Mulliken overlap populations (OPs) and ionic charges. The Ga–O distances differ from experiment [39] by <0.02 Å. The OPs are somewhat smaller than those found in Extended Hückel Theory results [41] which are in the range of 0.26–0.29 for Ga(I)–O and 0.14–0.23 for Ga(II)–O bonds. However, the general result that the Ga(I)–O bonds are more covalent is reproduced in the present calculations. The ionic charges are somewhat larger than those obtained [42] in tight-binding calculations, which give +1.80 and +1.64 for Ga(I) and Ga(II), respectively, and −1.09 to −1.18 for the O ions.

The bulk band structure of β-Ga_2O_3 has been studied theoretically by several groups [41–44]. The bulk valence band density of states was computed, using DFT with all-electron basis sets as described above, for the optimized lattice structure given in Table 1. The results (not shown) are in good agreement with previous work[5] [43] which used the FLAPW method with the Perdew–Wang exchange-correlation functional. The band structure was also obtained (not shown) and found to be in good agreement with previous work [43]. In particular a deep conduction band minimum (CBM) occurs at the Γ-point, and the valence band maximum (VBM) is nearly flat. The band gap obtained in the present work is $E_g = 5.09$ eV vs. experimental values in the range of 4.5–4.9 eV [29,45,46]. A calculated E_g that is somewhat larger than the observed value is typical [37] for the B3LYP functional.

3.2. The (1 0 0) surface

Fig. 1 indicates two possible (1 0 0) surface terminations, labeled "A" and "B", which correspond to stoichiometric unit cells with non-polar surfaces. These are described as follows.

A: terminated in rows of O(II)'s lying along the [0 1 0] direction with each O(II) back-bonded to two Ga(I)s. Between each O(II) row is a row of Ga(II) sites. The surface O(II) and Ga(II) atoms are each singly-unsaturated, i.e., missing a single nearest neighbor vs. the corresponding bulk sites. Ga(I), O(I) and O(III) atoms at the surface are fully coordinated, as in the bulk. This surface is formed by cleaving the Ga(II)–O(II) bonds shown in plane A in Fig. 1, while leaving the Ga(I)–O(II) bonds intact, which results in two identical cleavage surfaces.

[4] Fig. 1 was constructed using the VENUS set of programs (R.A. Dilanian and F. Izumi) obtained at http://homepage.mac.com/fujioizumi/visualization/VENUS.html.

[5] The convention used in [43] for labeling the O ions differs from that used here and in [39]. The O(2) [O(3)] of [43] is the O(III) [O(II)] of [39].

Table 2
Computed bulk nearest-neighbor distances, Mulliken overlap populations and ionic charges[a] for β-Ga_2O_3

	O(I)	O(II)	O(III)[b]	Charge
Ga(I)	1.822 (1) [0.169]	1.824 (2) [0.162]	1.850 (1) [0.150]	+2.080
Ga(II)	1.934 (2) [0.118]	1.932 (1) [0.116]	1.994 (1); 2.081 (2) [0.094]; [0.080]	+2.164
Charge	−1.412	−1.383	−1.449	

[a] Entries such as Ga(I)–O(I) are nearest-neighbor distances in Å. Values in parentheses are the numbers of nearest-neighbors of a given type, and charges are in units of $|e|$. Numbers in brackets are Mulliken overlap populations (OPs) for the pair of nearest-neighbor atoms. For example, Ga(I) has two O(II) nearest neighbors at a distance of 1.824 Å with a bond OP of 0.162, and the Ga(I) ionic charge is $+2.080|e|$.
[b] Each Ga(II) has one O(III) at 1.994 Å and two more at 2.081 Å. The shorter of the two Ga(II)–O(III) bond lengths corresponds to a slightly larger OP.

B: terminated in nearest-neighbor rows of Ga(II) and O(III) atoms, each singly-unsaturated. Ga(I) and O(I) atoms at the surface are fully coordinated, and there are no O(II) atoms in the surface plane.

These are both "Type 2" structures as defined by Tasker [47,48] in that each individual layer is charged, but the repeat unit (i.e., the unit cell) has no static dipole moment. Hence, the surface energy (see below) is expected to converge to a finite value with increasing slab thickness.

The (1 0 0) surface structures used in previous cluster calculations differ from those described above. Kohl et al. [31], in their investigation of CH_4 adsorption, used a surface like A but with a complete layer of O(II) atoms for which all Ga sites are fully coordinated.[6] This is a polar surface since, for a stoichiometric lattice, the corresponding $(\bar{1}\,0\,0)$ surface would be terminated in a layer composed of rows of doubly-unsaturated Ga(I) and singly-unsaturated Ga(II) sites (see Fig. 1). Gonzalez et al. [32], in their study of H adsorption, in fact used this polar Ga-terminated surface as model for a surface with O vacancies. In the absence of charge-compensating adsorbates or defects [47,48] this type of structure would not be expected to yield a finite surface energy.

The results for the (1 0 0)-A surface will be discussed first. The calculations were done using slabs of $N = 20$, 40 and 60 layers, where $N = 20$ corresponds to one crystallographic unit-cell distance in the [1 0 0] direction (cf. Fig. 1). The symmetry and stoichiometry of the bulk unit cell are thus preserved, and there is only one atom per layer in the primitive unit cell. In view of the results of Gomes et al. [49], the slabs were "cut" from the optimized bulk lattice described above, rather than from the experimental lattice. Geometry optimization was done globally, i.e., by allowing complete freedom of motion to all atoms in the slab. However, the symmetry of the unrelaxed slab was maintained so that displacements of corresponding atoms in layers m and $N - m + 1$ were the same. Relaxation of the whole slab (rather than of only the outermost layer or two) was done in view of the large displacements, extending several layers into the slab, that have been reported for Cr_2O_3 [50] and for various forms of Al_2O_3 [51–54]. A slab is considered sufficiently thick if the displacements thus generated become essentially zero in all directions as the middle of the slab is approached.

In this and in following sections, the effects of relaxation will be described in three complementary ways. First, plots of the atomic displacements along the surface normal and in the surface plane will be given vs. depth into the slab to show the magnitude of the effect and its extent into the bulk. Second, the displacements will be shown graphically, superimposed on the ideally-terminated unit cell. However, for clarity, only the outermost layer of each inequivalent atom type will be shown. Third, the effects on local bonding will be described in terms of ionic charges, nearest-neighbor distances and bond OPs relative to the corresponding bulk quantities.

Fig. 2 shows the displacements vs. layer number, starting from the surface plane ($m = 1$) and progressing into the bulk, for the optimized $N = 60$ slab. The displacements are defined with respect to the corresponding positions in the bulk lattice. One small tick mark on the vertical axis corresponds to 0.02 Å, or about 1% of a typical Ga–O nearest-neighbor distance (cf. Table 2). Thus, the effect of relaxation may be considered to be small for $m > \sim 10$ (i.e., about half-way into the outermost crystallographic unit cell). Fig. 3 shows the surface relaxation graphically. For clarity, the displacement vectors have been magnified by a factor of 4 relative to the interatomic distances.

The relaxation process is seen to be complex, with the outermost Ga(I) and O(I) atoms moving up toward the surface and the O(II) surface layer displacing laterally. However, there is little difference between the bulk and surface ionic charges which, for corresponding atom types, differ by $\leqslant 0.06|e|$ (cf. Table 2). As expected, the greatest difference between bulk and surface ion charges occurs for the unsaturated Ga(II) and O(II) sites which are slightly less ionic than in the bulk. Relative to the bulk (Table 2), the Ga(I)–O(I) and Ga(I)–O(III) distances are longer (1.911 and 2.027 Å, respectively) and the Ga(I)–O(II) distance shorter (1.720 Å). The Ga(II)–O(I) distance is virtually unchanged (1.932 Å) while the Ga(II)–O(III) distances are slightly shorter (1.946 and 2.024 Å). Thus, the Ga(I) tetrahedron appears to be more

[6] The notation in [31] differs from that used here. Surface O atoms are labeled "O(I)" and "O(II)" according to the type of Ga site to which they are bonded. However (cf. Fig. 1) all surface O atoms in this model are properly termed "O(II)" in the present usage.

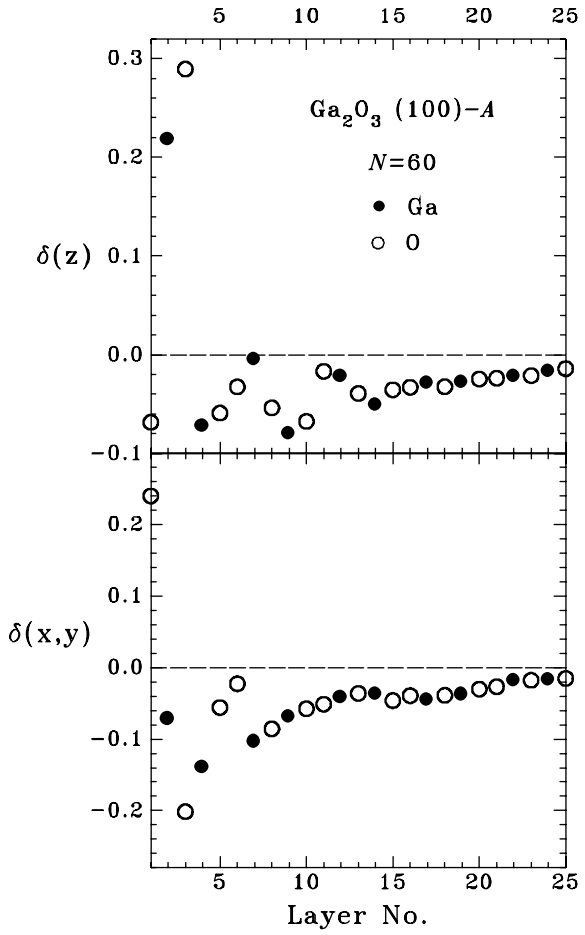

Fig. 2. Displacements (in Å), vs. layer number, along the surface normal [$\delta(z)$] and in the surface plane [$\delta(x,y)$] relative to the ideally-terminated positions for the (1 0 0)-A surface. The results are those computed for a fully-relaxed $N = 60$ slab. Layer number 1 is the outermost surface layer, and $\delta(z) > 0$ corresponds to an outward displacement.

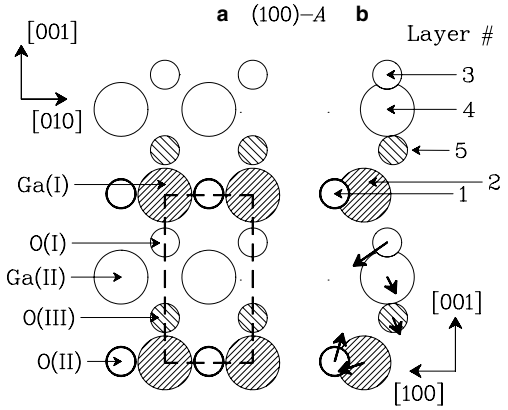

Fig. 3. Schematic model of the ideally-terminated (1 0 0)-A surface. (a) The view along the surface normal with the dashed lines indicating the surface unit cell. For simplicity, only the outermost layer of each type (O(I), Ga(I), etc.) is shown. (b) The outermost surface layers, viewed along the [0 1 0] direction, with vectors indicating the displacements occurring during relaxation. For clarity, the displacement vectors have been magnified by a factor of 4 relative to the interatomic distances. All displacements are in the plane of the page, i.e., the (0 1 0) plane. For simplicity, displacements of translationally-equivalent atoms, which are identical to those shown, have been omitted.

distorted on the relaxed surface than in the bulk. Qualitatively, the OPs increase, vs. the bulk values, as the bond distances decrease.

The surface energy of a two-dimensionally-periodic slab with a thickness of K primitive unit cells, σ_K, is defined as [51] $E(K) = 2A\sigma_K + KE_B$, where $E(K)$ is the total energy per slab unit cell, E_B is the energy per unit cell of the bulk and A is the area of the slab unit cell. Both faces of the slab are taken to be identical. The practical difficulties in obtaining a converged value, $\sigma = \sigma_K$ $(K \to \infty)$, and in choosing a self-consistent E_B are discussed elsewhere [55]. In the present work, $E(K)$ was computed in single-point DFT calculations for both ideal and globally-relaxed slabs (see above) with $N = 20$, 40 and 60 (i.e., $K = 2$, 4 or 6 primitive unit cells) and found to be linear vs. K over this range, which implies that convergence is achieved for $N \geqslant 20$. A value for σ (either ideally-terminated or relaxed) was then obtained from the zero-intercept of the linear least-squares fit, and the results are given in Table 3.

The calculations described thus far are based on a (1×1) surface unit cell. To determine whether the inclusion of longer-range interactions would yield a further lowering of energy, a calculation was done for an $N = 20$ slab with a (2×2) unit cell. This allows for the possibility of reconstruction as well as relaxation. However, the optimized RHF/pseudopotential total energy of the fully-relaxed (2×2) structure differed from that of the (1×1) by less than 1 meV per (1×1) slab unit cell. Hence, the surface structure is adequately modeled with the (1×1) unit cell.

Similar calculations were done for a (1×1) unit cell with the (1 0 0)-B termination, and the results are shown in Figs. 4 and 5. The surface energy is even lower for this structure than for the (1 0 0)-A. The displacements of atoms for the (1 0 0)-B are generally smaller in magnitude than are those of corresponding atoms for the (1 0 0)-A, which is consistent with (1 0 0)-B being the more stable of the two before relaxation. Also, the $\delta(z)$ values indicate a predominantly inward displacement of atoms near the (1 0 0)-B surface. The fact that the relaxed (1 0 0)-B surface has the lowest energy of those considered here (cf. Table 3) is consistent with the observation [15,16] that β-Ga_2O_3 cleaves easily

Table 3
Surface energies (σ, J m^{-2}) for the ideally-terminated and the relaxed or reconstructed surfaces

	Area	Ideal σ	Relaxed σ
(1 0 0)-A	0.1760	1.68	1.13[a]
(1 0 0)-B		0.96	0.68[a]
(0 1 0)	0.6874	2.78	2.03[a]
(0 0 1)-A	0.1852	3.35	
(0 0 1)-B		2.65	1.40[b]
(1 0 $\bar{1}$)	0.3705	3.99	1.57[a]

The area (nm^2) is that of the primitive (1×1) surface unit cell. The labels "A" and "B" refer to different lattice terminations.

[a] Relaxed (1×1) unit cell. 1 eV nm^{-2} = 0.160219 J m^{-2}.

[b] Reconstructed (2×2) unit cell. A minimum-energy configuration could not be located by relaxing a (1×1) unit cell (see text).

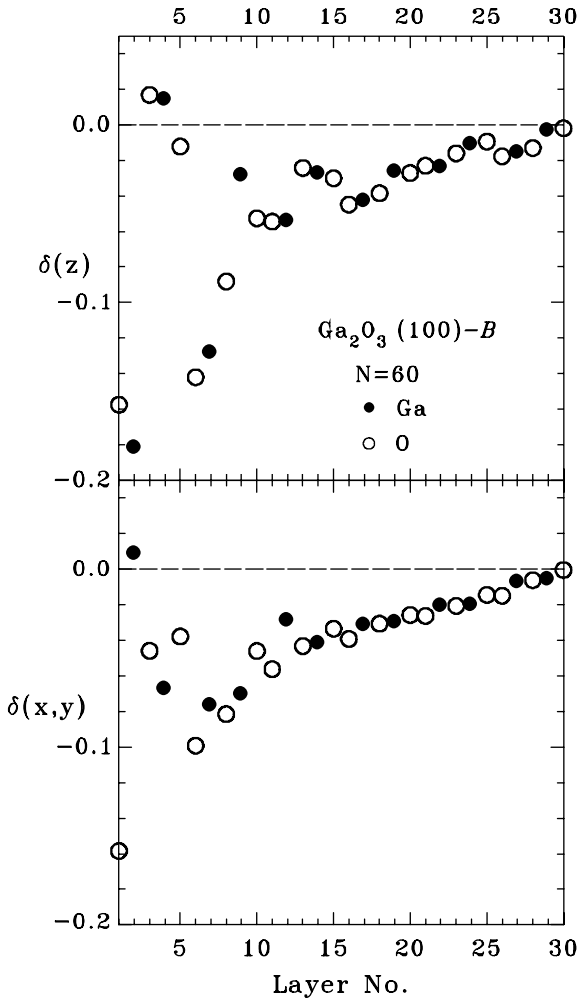

Fig. 4. Similar to Fig. 2 but showing results for the (1 0 0)-B surface.

on the (1 0 0) plane. The (1 0 0)-B surface[7] is also the one proposed [24,28,29] for crystalline β-Ga_2O_3 films formed by oxidation of CoGa (1 0 0) and (0 0 1) surfaces. It has also been noted [9] that β-Ga_2O_3 nanoribbons grow with (1 0 0) as the broad surface which is consistent with the relatively low σ for the (1 0 0)-B. The greater stability of the (1 0 0)-B vs. -A surface is probably due to the lesser degree of unsaturation for the former. On (1 0 0)-B the surface O(III) atoms are missing one out of four Ga nearest-neighbors; whereas, on (1 0 0)-A the surface O(II) atoms are missing one out of three bulk nearest-neighbor Ga atoms.

In terms of local bonding, the relaxed (1 0 0)-B surface differs only slightly from the bulk which is consistent with its relatively low σ. The surface ionic charges differ from those in the bulk by $\leqslant 0.05|e|$. The Ga(I)–O(I) and Ga(I)–O(II) distances (1.843 and 1.839 Å, respectively) are slightly larger than in the bulk, and the Ga(I)–O(III) distance is

[7] The definition of the crystal axes used in [24,28,29] differs from that in [39,40] and in the present work. The axes *a*, *b*, *c* in the former correspond to the axes *b*, *c*, *a* in the latter. Hence, the (0 0 1) plane described in [24,28,29] is the (1 0 0) plane of the present work.

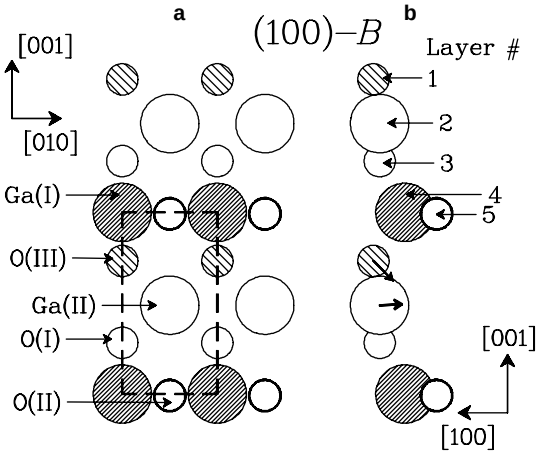

Fig. 5. Similar to Fig. 3 but showing results for the (1 0 0)-B surface. In (a), only Ga(II) and O(III) exhibit a significantly large relaxation displacement. Other displacements are too small to be seen clearly, even when magnified, and have been omitted from (b).

slightly smaller (1.844 Å), indicating a more regular tetrahedron at the surface. The Ga(II)–O(I) distance (1.978 Å) is slightly greater than in the bulk, and the Ga(II)–O(II) distance is slightly smaller (1.887 Å). The distance from Ga(II) to the two equidistant O(III) sites is 1.974 Å, slightly less than the bulk value of 2.081 Å.

3.3. The (0 1 0) surface

For this surface there is only one termination, which contains all five atom types with two Ga_2O_3 units per surface unit cell per slab layer. Thus, the (0 1 0) orientation involves 10 atoms per layer unlike the (1 0 0), discussed above, with only one atom per layer. Figs. 6 and 7 give the structural results for this surface, which can be described as follows:

[*Ga(I)*:] bonded to one O(I) and one O(III) in plane; one O(II) below.
[*Ga(II)*:] bonded to one O(II) and one O(III) in plane; one O(I) and one O(III) below.
[*O(I)*:] bonded to one Ga(I) in plane; one Ga(II) below.
[*O(II)*:] bonded to one Ga(II) in plane; one Ga(I) below.
[*O(III)*:] bonded to one Ga(I) and one Ga(II) in plane; one Ga(II) below.

All surface atoms are singly-unsaturated except for the Ga(II) which is doubly-unsaturated. The surface layer may be viewed (Fig. 7(a)) as consisting of individual Ga_2O_3 units back-bonded to underlayer atoms, with no direct interaction between surface Ga_2O_3 units.

Global geometry optimizations were performed for $N = 5$, 7, 11 and 15 with convergence being achieved, as defined above, for $N \geqslant 7$. The displacements obtained for $N = 15$ are given in Figs. 6 and 7(b), and the surface energies for the ideal and the relaxed slabs are listed in Table 3. The effect of relaxation is seen to be small, as defined

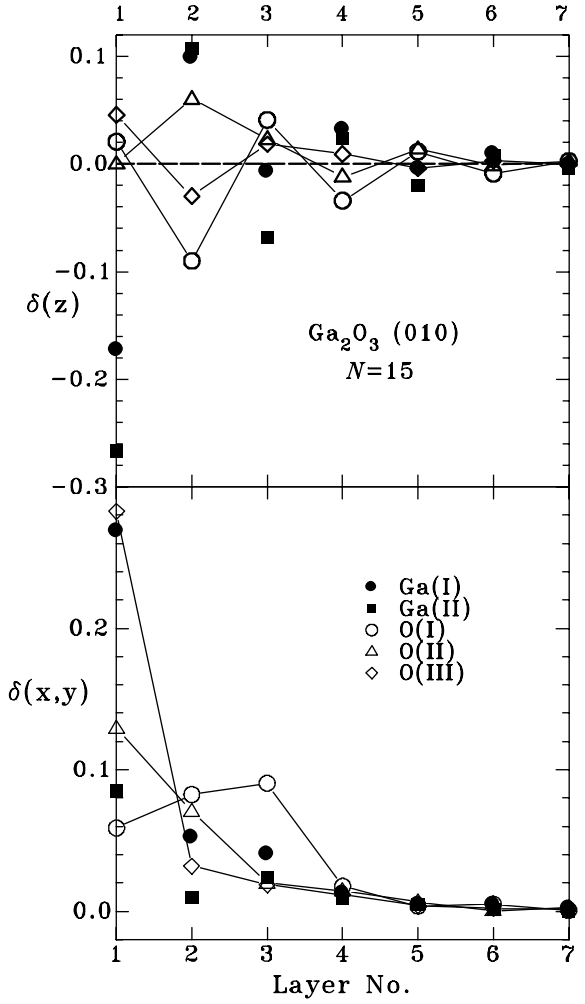

Fig. 6. Similar to Fig. 2 but showing results for the (0 1 0) surface for an $N = 15$ slab. The "$\delta(x,y)$" quantity plotted in this case is $(\delta(x)^2 + \delta(y)^2)^{1/2}$. Lines connecting the O points are visual aids.

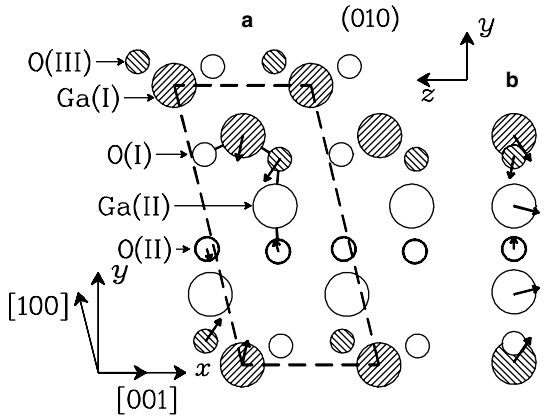

Fig. 7. Similar to Fig. 3 but showing the (0 1 0) surface. In (a), heavy lines connecting a few of the atoms illustrate the surface bonding described in the text. In (b), all atoms shown are in the same (outermost) plane for the ideally-terminated surface. The O(I) displacements are too small to be seen clearly.

above, beyond the third or fourth layer into the bulk of the slab, where three layers correspond to one crystallographic unit cell distance in the [0 1 0] direction. The surface ionic charges were found to be somewhat smaller than in the bulk, indicating a higher covalency at the surface. The relaxed $N = 15$ (0 1 0) surface charges were (cf. Table 2) $+2.017|e|$ and $+2.091|e|$ for Ga(I) and Ga(II), respectively, and $-1.358|e|$, $-1.336|e|$ and $-1.377|e|$ for O(I), O(II) and O(III), respectively. At the surface, the distances from Ga(I) to O(I), O(II) and O(III) (1.707, 1.803 and 1.762 Å, respectively) are all shorter than in the bulk, with correspondingly larger OPs. Likewise, the distances from Ga(II) to O(I) and O(II) (1.879 and 1.754 Å) are shorter, with larger OPs, than in the bulk. At the surface, there are two unequal Ga(II)–O(III) bonds which are again shorter (1.847 and 1.910 Å) than in the bulk. The results indicate an increased covalent interaction between pairs of surface atoms so that the (0 1 0) surface resembles to some extent a layer of Ga_2O_3 "molecules" chemisorbed on the surface of the bulk lattice.

As in the case of the (1 0 0)-A surface discussed above, a geometry optimization was also done for an $N = 5$ slab with a (2×2) supercell (containing a total of 200 atoms per slab unit cell) in order to determine if reconstruction would further lower the total energy of the relaxed structure. However, the RHF/pseudopotential energy of the fully-relaxed (2×2) structure differed from that of the (1×1) by less than 1 meV per (1×1) slab unit cell.

3.4. The (0 0 1) surface

As in the case of the (1 0 0), two non-polar (0 0 1) terminations of the stoichiometric unit cell are possible.

A: terminated in rows of singly-unsaturated O(I) atoms lying along the [0 1 0] direction and back-bonded to two Ga(II)s. The O(I) rows are separated by rows of singly-unsaturated Ga(I)s. Ga(II) and O(II) atoms in the surface plane are fully coordinated, and there are no O(III)s in the plane.

B: terminated in rows of doubly-unsaturated O(III) atoms back-bonded to one Ga(I) and one Ga(II) and separated by rows of doubly-unsaturated Ga(II) sites. Ga(I) and O(II) atoms in the surface plane are fully coordinated, and there are no O(I)s in the surface plane.

When relaxing (1×1) unit cells for either termination a minimum-energy configuration, in which the forces on all atoms are effectively zero, could not be located. The behavior during optimization suggests that the potential energy surface is relatively flat near the energy minimum, and increasing the precision limits for SCF convergence and for the truncation of the Coulomb and exchange terms (see above) did not rectify the situation. However, convergence was achieved by increasing the slab unit cell from (1×1) to (2×2). In view of the large number of atoms involved (e.g., 160 atoms for a (2×2) $N = 40$ slab), only the B termination was considered since σ for the ideally-terminated (0 0 1)-B is significantly lower than that of the

(0 0 1)-A (Table 3). Thus it is assumed that the (0 0 1)-B will remain the lower of the two in energy even for a (2×2) surface unit cell. The results for the (0 0 1)-B (2×2) surface are shown in Figs. 8 and 9. The distinction between the (2×2) and (1×1) surface unit cells is very small, in that there are only slight differences (<0.0 0 1 Å) in the displacements of atoms in the (2×2) cell that are translationally equivalent in the (1×1). Hence, there is little or no indication of an actual reconstruction, and Fig. 9 shows only the (1×1) cell.

The charges on the doubly-unsaturated surface Ga(II) and O(III) ions (+2.063|*e*| and −1.317|*e*|, respectively) are smaller in magnitude by ~0.1|*e*| than on the corresponding bulk ions (cf. Table 2), indicating a higher degree of covalency. However, the charges on the other surface ions differ by at most 0.016|*e*| from the bulk counterparts. The Ga(I)–O(I) and Ga(I)–O(III) distances (1.799 and 1.765 Å, respectively) are shorter than in the bulk; whereas, the Ga(I)–O(II) distance is longer (1.885 Å). Thus, the Ga(I) tetrahedron is more distorted than in the bulk. The Ga(II)–O(I) and Ga(II)–O(II) distances (1.837 and 1.900 Å, respectively) are both shorter than in the bulk.

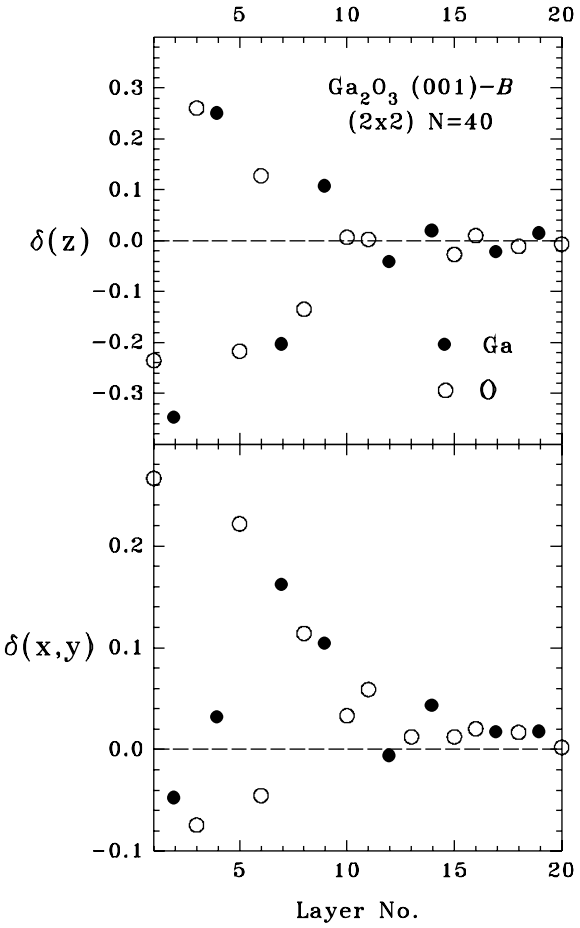

Fig. 8. Similar to Fig. 2 but showing results for the (0 0 1)-B (2×2) surface for an $N=40$ slab. As noted in the text, the (2×2) surface unit cell was used as a means of promoting convergence of the geometry optimization, but there is little or no indication of an actual reconstruction.

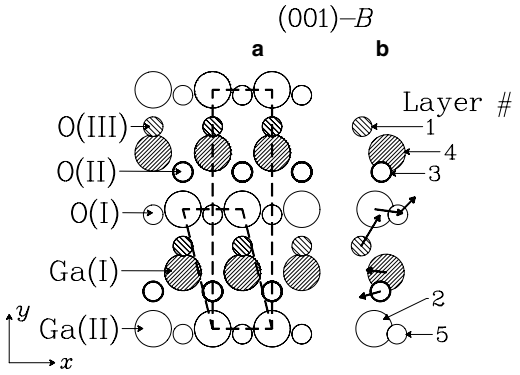

Fig. 9. Similar to Fig. 3 but showing results for the (0 0 1)-B surface. Only the (1×1) primitive and crystallographic surface unit cells are shown (see text). The Ga(II) and O(III) surface sites are each doubly-unsaturated (i.e., missing two of the bulk nearest-neighbors). All other species are fully coordinated.

The one Ga(II)–O(III) bond is much shorter than in the bulk (1.748 vs. 1.994 Å) with a much higher OP (0.205 vs. 0.094, cf. Table 1). Thus, the Ga(II) is more covalently bonded at the surface than in the bulk.

3.5. The $(1\,0\,\bar{1})$ surface

The $(1\,0\,\bar{1})$ surface was also analyzed in view of its importance, noted above, in the growth of β-Ga_2O_3 nanoribbons. This surface consists of (cf. Fig. 1) rows of doubly-unsaturated O(I) and singly-unsaturated O(III) atoms lying along the [0 1 0] direction. A row of singly-unsaturated Ga(I) sites lies adjacent to the O(I) row, and a row of doubly-unsaturated Ga(II) sites lies adjacent to the O(III) row. The surface O(II) atoms are fully coordinated. In forming the surface, Ga(I) loses its O(III) bulk nearest-neighbor, and Ga(II) loses its two O(I) bulk nearest-neighbors (cf. Fig. 1).

Global geometry optimizations were done for $N=20$, 40, 60 and 80, with convergence being achieved for $N\geqslant40$. The displacements obtained for $N=80$ are shown in Figs. 10 and 11. In this case, relaxation results in larger displacements near the surface than were found for other planes; however, these become negligibly small beyond $m\approx20$. The surface energy of the ideally-terminated surface (Table 3) is relatively high, as expected from the high degree of unsaturation noted above. Relaxation yields a substantial reduction in σ, by a factor of ~2.5, which is a larger effect than for any other surface studied here. The relaxation is also accompanied by a larger redistribution of ionic charges than was noted for other surfaces. Table 4 shows the nearest-neighbor distances, OPs and ionic charges for the $(1\,0\,\bar{1})$ surface in the same format as those for the bulk given in Table 2. As was done for other surfaces, a calculation was performed for a (2×2) surface unit cell (with $N=40$), and a negligible effect on the total energy was again found.

The origin of the remarkable stabilization of the $(1\,0\,\bar{1})$ surface can be seen by comparing Tables 2 and 4 and by

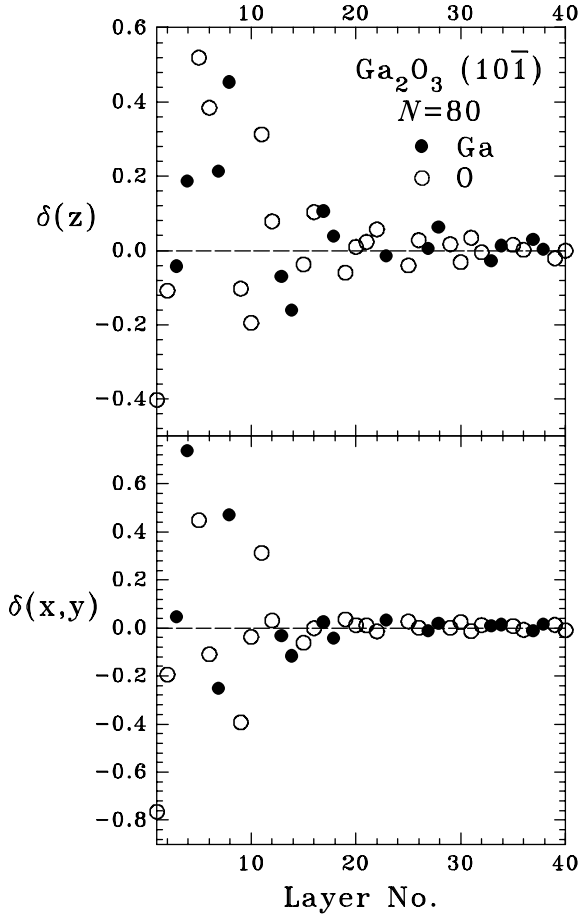

Fig. 10. Similar to Fig. 2 but showing results for the (1 0 $\bar{1}$) surface for an $N = 80$ slab. Note the much larger magnitudes for displacements near the surface in comparison to Figs. 2, 4, 6 and 8.

examining Fig. 11. Fig. 11 is only indicative, however, since underlayer atoms, which also undergo significant displacements (cf. Fig. 10), have been omitted for clarity. As noted above, Ga(I) and O(I) are singly- and doubly-unsaturated, respectively, on the ideally-terminated surface. However, relaxation results in displacement of O(I) and Ga(I) towards each other to form a "bulk-like" bond (OP = 0.101), leaving the O(I) fully coordinated and the Ga(I) fivefold coordinated (vs. fourfold in the bulk). This in turn leads to a weakening of the Ga(I)–O(II) bond (i.e., a decrease in OP from 0.162 in the bulk to 0.125 at the surface) and a strengthening of the Ga(II)–O(II) interaction (i.e., an increase in OP from 0.116 to 0.154). The Ga(II)–O(III) interaction at the surface is also noticeably stronger than in the bulk.

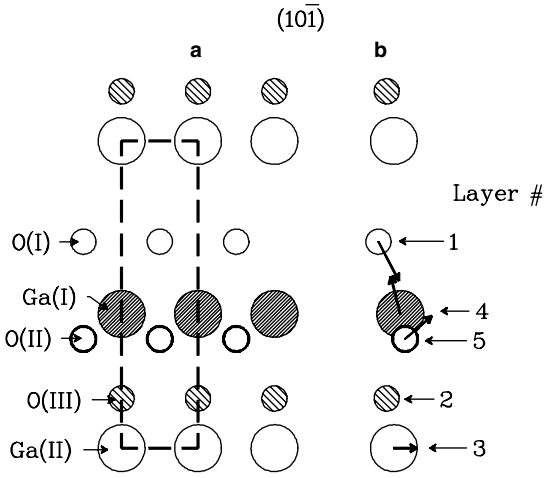

Fig. 11. Similar to Fig. 3 but showing results for the (1 0 $\bar{1}$) surface. The displacement vectors have been magnified by a factor of 2 relative to the interatomic distances. Note that in corresponding figures for other surfaces the magnification is by a factor of 4. The O(III) displacement is too small to be seen clearly.

3.6. The (1 0 0) surface electronic structure

As noted previously, bulk single crystals of β-Ga_2O_3 cleave easily on the (1 0 0) plane [15,16]. Hence, it should be possible to observe experimentally the electronic structure of this surface by cleaving a crystal in ultra-high vacuum (UHV) and obtaining ultraviolet photoemission spectroscopy (UPS) data. Charging of the insulating sample during UPS could be eliminated by first annealing in UHV to create oxygen vacancies, thus inducing n-type semiconductor behavior [56]. A UPS experiment of this nature has not, to our knowledge, been reported yet. It is also noted that the (1 0 0)-B structure has been proposed for crystalline β-Ga_2O_3 films grown by oxidation of CoGa(1 0 0) and (0 0 1) surfaces [24,29]; although, again, no UPS data have been reported.

In order to examine the possibility of intrinsic surface states, the surface band structure was computed for the fully-relaxed (1×1) $N = 60$ slab with the (1 0 0)-B structure, and the results (near the band edges) are shown in Fig. 12. The surface Brillouin zone, which is simple for the (1 0 0) plane, was constructed using the monoclinic reciprocal lattice vectors given by Hunderi [57]. The results show basically the same nearly-flat VBM and deep CBM at Γ as is seen for the bulk [43], and there is no indication of surface-related features in the band gap. The absence of intrinsic surface states near the VBM should assist in the

Table 4
Similar to Table 2 but showing results for the relaxed (1 0 $\bar{1}$) surface

	O(I)	O(II)	O(III)	Charge
Ga(I)	1.852 (1); 2.067 (2) [0.189]; [0.101]	1.989 (2) [0.125]		+2.118
Ga(II)		1.938 (1) [0.154]	1.848 (1); 2.072 (2) [0.178]; [0.110]	+2.056
Charge	−1.387	−1.391	−1.346	

See text for details.

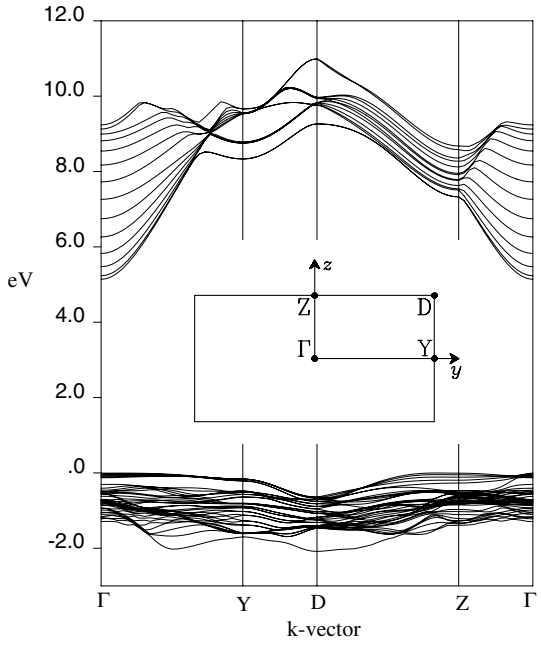

Fig. 12. Surface band structure diagram, computed using DFT with all-electron basis sets, for the fully-relaxed (1×1) $N = 60$ slab with the (1 0 0)-B termination. The inset shows the surface Brillouin zone. The region shown comprises the upper (lower) part of the valence (conduction) band, and the zero of energy is at the valence band maximum. The y-axis lies parallel to the [0 1 0] direction.

detection and identification of extrinsic surface states arising from defects. In their electron energy loss data for β-Ga_2O_3 (1 0 0) films on CoGa, Schmitz et al. [29] reported a peak of uncertain origin at 3.3 eV in addition to the interband transition at about 4.5 eV. The present results indicate that the 3.3 eV feature is not associated with intrinsic surface states.

4. Summary

In conclusion, the physical and electronic structure of the (1 0 0), (0 1 0), (0 0 1) and $(1\ 0\ \bar{1})$ faces of β-Ga_2O_3 have been addressed using ab initio theory. For the bulk, good agreement is obtained with available experimental data (i.e., crystal structure and band gap) and with previous ab initio studies (i.e., band structure). The results provide a physical picture of the structure of each surface and of how that structure is derived by relaxing the corresponding ideally-terminated surface. In all cases, especially for the $(1\ 0\ \bar{1})$ plane, large displacements from the ideal positions are found for atoms near the surface; however, such effects decay quickly with distance into the bulk.

The stability of various surface planes and terminations has been assessed via calculation of the respective surface energies. The relatively low σ of the (1 0 0)-B surface is consistent with the observed tendency of β-Ga_2O_3 single crystals to cleave on the (1 0 0) plane and with the tendency of β-Ga_2O_3 nanoribbons to grow with the (1 0 0) plane as the wide surface. Growth with this structure allows nanoribbon formation to proceed with a minimal increase in surface energy. The stability of the (1 0 0)-B surface is ascribed to a local bonding configuration that is not very different from that of the bulk.

For growth in the [0 0 1] direction, the narrow face of the nanoribbon is the more energetic (0 1 0) plane. The local bonding on the (0 1 0) surface is found to resemble somewhat that of a layer of chemisorbed Ga_2O_3 "molecules". However, growth in the [0 1 0] direction occurs with $(1\ 0\ \bar{1})$, and not (0 0 1), as the narrow face. This is at first surprising, in view of the high σ of the ideally-terminated $(1\ 0\ \bar{1})$ surface. However, Table 3 shows that relaxation leads to a very substantial reduction in σ for the $(1\ 0\ \bar{1})$, to a value only ~12% larger than that of the (0 0 1)-B. The stabilization of the $(1\ 0\ \bar{1})$ is analyzed in terms of a significant reconfiguration of the local bonding at the relaxed surface. It is possible that some lesser effect not considered here, such as defect formation, further stabilizes the $(1\ 0\ \bar{1})$ to a point where it is energetically favored over the (0 0 1) as the narrow ribbon face.

Of the surfaces considered, the most stable structures (i.e., (1 0 0)-B, (1 0 0)-A and (0 0 1)-B, in order of increasing σ) all have unsaturated Ga(II) sites but no unsaturated Ga(I) sites. This is in apparent conflict with experimental results [17] for Ga_2O_3 powders which indicate essentially equivalent bulk and surface compositions. For β-Ga_2O_3 this means that the powder surface has, on average, nearly equal concentrations of unsaturated Ga(I) and Ga(II) sites. One factor could be the tendency to form O vacancies during heating in vacuo [56], which is done to prepare clean Ga_2O_3 powder surfaces [17]. However, an impossibly high concentration of such vacancies would be needed to account, by this means alone, for the experimental observation. Another possibility is that the $(1\ 0\ \bar{1})$ surface, which has equal concentrations of unsaturated Ga(I) and Ga(II), might be favored for β-Ga_2O_3 in the form of small particles as it is for nanoribbons grown in the [0 1 0] direction. A further possibility is that, for example, the polar (1 0 0) surface termination consisting of a layer of unsaturated Ga(I) and Ga(II) sites [32] might be stabilized on powder surfaces by the formation of charge-compensating defects [48].

Acknowledgements

This work was supported by the Office of Naval Research and by a grant of computer time from the DOD High-Performance Computing Modernization Program at the ASC-MSRC, Wright-Patterson AFB. C. McGuinness is thanked for pointing out the existence of the VENUS program for lattice modeling, and Z. Hajnal and J. Pollmann are thanked for helpful communications.

References

[1] M. Orita, H. Hiramatsu, H. Ohta, M. Hirano, H. Hosono, Thin Solid Films 411 (2002) 134.
[2] M. Fleischer, J. Giber, H. Meixner, Appl. Phys. A 54 (1992) 560.

[3] F. Becker, Ch. Krummel, A. Freiling, M. Fleischer, C. Kohl, Fresenius J. Anal. Chem. 358 (1997) 187.
[4] T. Schwebel, M. Fleischer, H. Meixner, C.-D. Kohl, Sens. Actuat. B 49 (1998) 46.
[5] M. Ogita, K. Higo, Y. Nakanishi, Y. Hatanaka, Appl. Surf. Sci. 175–176 (2001) 721.
[6] Z.L. Wang, Ann. Rev. Phys. Chem. 55 (2004) 159.
[7] H.W. Kim, N.H. Kim, Acta Phys. Polon. A 107 (2005) 346.
[8] N.H. Kim, H.W. Kim, Appl. Surf. Sci. 242 (2005) 29.
[9] Z.R. Dai, Z.W. Pan, Z.L. Wang, J. Phys. Chem. B 106 (2002) 902.
[10] H.W. Kim, N.H. Kim, Appl. Surf. Sci. 233 (2004) 294.
[11] G.-S. Park, W.-B. Choi, J.-M. Kim, Y.C. Choi, Y.H. Lee, C.-B. Lim, J. Crystal Growth 220 (2000) 494.
[12] J. Zhang, F. Jiang, L. Zhang, Phys. Lett. A 322 (2004) 363.
[13] P. Guha, S. Chakrabarti, S. Chaudhuri, Physica E 23 (2004) 81.
[14] H.W. Kim, N.H. Kim, Appl. Phys. A 80 (2005) 537.
[15] Y. Tomm, P. Reiche, D. Klimm, T. Fukuda, J. Cryst. Growth 220 (2000) 510.
[16] E.G. Víllora, Y. Murakami, T. Sugawara, T. Atou, M. Kikuchi, D. Shindo, T. Fukuda, Mater. Res. Bull. 37 (2002) 769.
[17] S.E. Collins, M.A. Baltanás, A.L. Bonivardi, Langmuir 21 (2005) 962.
[18] R. Rodríguez Delgado, C. Otero Areán, Mater. Lett. 57 (2003) 2292.
[19] F. Bozon-Verduraz, C. Potvin, J. Chim. Phys. 73 (1976) 43.
[20] O.O. Parenago, Yu.N. Pushkar', A.O. Turakulova, G.P. Murav'eva, E.V. Lunina, Kinet. Katal. 39 (1998) 288, English trans.: Kinet. Catal. 39 (1998) 268.
[21] P. Chen, R. Zhang, X.F. Xu, Y.G. Zhou, Z.Z. Chen, S.Y. Xie, W.P. Li, Y.D. Zheng, Appl. Phys. A 71 (2000) 191.
[22] S.D. Wolter, S.E. Mohney, H. Venugopalan, A.E. Wickenden, D.D. Koleske, J. Electrochem. Soc. 145 (1998) 629.
[23] C. Tang, Y. Bando, Z. Liu, Appl. Phys. Lett. 83 (2003) 3177.
[24] R. Franchy, M. Eumann, G. Schmitz, Surf. Sci. 470 (2001) 337.
[25] F.M. Pan, Ch. Pflitsch, R. David, L. Verheij, R. Franchy, Surf. Sci. 478 (2001) 191.
[26] F.M. Pan, Ch. Pflitsch, R. David, L. Verheij, R. Franchy, Surf. Sci. 490 (2001) L609.
[27] F.M. Pan, L.K. Verheij, R. David, R. Franchy, Thin Solid Films 400 (2001) 22.
[28] R. Franchy, Surf. Sci. Rep. 38 (2000) 195.
[29] G. Schmitz, P. Gassmann, R. Franchy, J. Appl. Phys. 83 (1998) 2533.
[30] M. Eumann, G. Schmitz, R. Franchy, Appl. Phys. Lett. 72 (1998) 3440.
[31] D. Kohl, T. Ochs, W. Geyer, M. Fleischer, H. Meixner, Sens. Actuat. B 59 (1999) 140.
[32] E.A. Gonzalez, P.V. Jasen, A. Juan, S.E. Collins, M.A. Baltanás, A.L. Bonivardi, Surf. Sci. 575 (2005) 171.
[33] J.C. Lavalley, M. Daturi, V. Montouillout, G. Clet, C. Otero Areán, M. Rodríguez Delgado, A. Sahibed-dine, Phys. Chem. Chem. Phys. 5 (2003) 1301.
[34] V.R. Saunders, R. Dovesi, C. Roetti, R. Orlando, C.M. Zicovich-Wilson, N.M. Harrison, K. Doll, B. Civalleri, I. Bush, Ph. D'Arco, M. Llunell, CRYSTAL2003 User's Manual, University of Torino, Torino, 2003.
[35] C. Pisani, R. Dovesi, C. Roetti, Hartree–Fock Ab Initio Treatment of Crystalline Systems, Springer, Berlin, 1988.
[36] I. Batyrev, A. Alavi, M.W. Finnis, Faraday Discuss. 114 (1999) 33.
[37] J. Muscat, A. Wander, N.M. Harrison, Chem. Phys. Lett. 342 (2001) 397.
[38] W.F. Perger, Chem. Phys. Lett. 368 (2003) 319.
[39] S. Geller, J. Chem. Phys. 33 (1960) 676.
[40] J. Åhman, G. Svensson, J. Albertsson, Acta. Cryst. C52 (1996) 1336.
[41] L. Binet, D. Gourier, C. Minot, J. Solid State Chem. 113 (1994) 420.
[42] E.A. Albanesi, S.J. Sferco, I. Lefebvre, G. Allan, G. Hollinger, Phys. Rev. B 46 (1992) 13260.
[43] K. Yamaguchi, Solid State Commun. 131 (2004) 739.
[44] Z. Hajnal, J. Miró, G. Kiss, F. Réti, P. Deák, R.C. Herndon, J.M. Kuperberg, J. Appl. Phys. 86 (1999) 3792.
[45] H. Ueda, H. Hosono, R. Waseda, H. Kawasoe, Appl. Phys. Lett. 71 (1997) 933.
[46] M. Orita, H. Ohta, M. Hirano, H. Hosono, Appl. Phys. Lett. 77 (2000) 4166.
[47] P.W. Tasker, J. Phys. C 12 (1979) 4977.
[48] C. Noguera, J. Phys.: Condens. Matter 12 (2000) R367.
[49] J.R.B. Gomes, I.P.R. de Moreira, P. Reinhardt, A. Wander, B.G. Searle, N.M. Harrison, F. Illas, Chem. Phys. Lett. 341 (2001) 412.
[50] C. Rehbein, N.M. Harrison, A. Wander, Phys. Rev. B 54 (1996) 14066.
[51] H.P. Pinto, R.M. Nieminen, S.D. Elliot, Phys. Rev. B 70 (2004) 125402.
[52] C. Ruberto, Y. Yourdshahyan, B.I. Lundqvist, Phys. Rev. Lett. 88 (2002) 226101.
[53] K. Sohlberg, S.J. Pennycook, S.T. Pantelides, J. Am. Chem. Soc. 121 (1999) 10999.
[54] R. DiFelice, J.E. Northrup, Phys. Rev. B 60 (1999) R16287.
[55] V. Fiorentini, M. Methfessel, J. Phys.: Condens. Matter 8 (1996) 6525.
[56] T. Harwig, G.J. Wubs, G.J. Dirksen, Solid State Commun. 18 (1976) 1223.
[57] O. Hunderi, J. Phys. F 5 (1975) 883.